Threshold Electron-Impact Ionization Mechanism for Hydrogen Atoms

J. F. Williams,[1] Philip L. Bartlett,[2] and Andris T. Stelbovics[2]

[1]*Centre for Atomic, Molecular and Surface Physics, University of Western Australia, Perth 6009, Australia*
[2]*The ARC Centre for Antimatter Matter Studies, Murdoch University, Perth 6150, Australia*

(Received 7 December 2005; published 27 March 2006)

The near-threshold evolution of electron-impact ionization of hydrogen is revealed with measurements of the angular and energy correlations of the outgoing electrons down to 0.05 eV. The single-, double-, and triple-differential cross sections in the perpendicular plane are measured simultaneously using a dual wedge-and-strip detector on a single-toroidal energy analyzer, avoiding many experimental problems. The experimental and calculated data are in excellent agreement, within the experimental precision of $\pm 10\%$, and provide further evidence that the accurate solution of the Schrödinger equation provides a complete description of the reaction dynamics of near-threshold ionization.

DOI: 10.1103/PhysRevLett.96.123201 PACS numbers: 34.80.Dp

A knowledge of ionization phenomena has traditionally been required in areas such as astrophysics, atmospheric physics, and plasma physics, and recent studies have shown that very low-energy electron-impact ionization is also important in biomolecular processes [1]. However, ionization experiments close to the ionization threshold are constrained by the measurement precision of the very low-energy breakup fragments. This Letter describes angular correlation measurements for a fundamental ionizing collision system that reduces this detection limit to 0.05 eV.

The electron impact of atomic hydrogen (e-H) is the simplest ionizing collision system and is more amenable to theoretical studies than multielectron targets. However, the challenges in producing an atomic hydrogen beam make the measurements difficult. Consequently, ionization threshold measurements of angular correlation using helium targets have been largely preferred (see [2]). At higher energies an understanding of e-H ionization has been established from momentum transfer dynamics which have been measured, precisely and then absolutely (see [3–5], for example). However, all measurements of the angular correlation of e-H ionizing collisions have been made in the coplanar geometry. Out-of-plane kinematics, while producing smaller cross sections, are known to be a stringent test of theoretical models [6,7].

The model of Wannier [8] is commonly used to predict the ionizing behavior of neutral atomic targets near the ionization threshold. The Wannier threshold law gives the total ionization cross section (TICS) as a function of excess energy above the ionization threshold as $\sigma \propto E^{1.127}$, though alternate theories have been proposed (e.g., [9]). Near-threshold studies [2,10–12] have shown that there is no preferred energy distribution between the escaping electrons and that the electron-pair angular correlations have a Gaussian distribution with a maximum at electron separations of $\phi_{12} = 180°$ and a full width at half maximum proportional to $E^{0.25}$. Accurate and complete numerical solutions of the underlying Schrödinger equation for e-H collisions has now been demonstrated using exterior complex scaling [13], and a recent Letter [14] has given the first *ab initio* numerical quantum-mechanical support for these threshold laws for hydrogen targets, suggesting that the Wannier region for hydrogen extends to about 2 eV above the ionization threshold. It is known that angular correlation measurements provide the most rigorous test for theory [6,15], and while these threshold laws are independent of the target, there is evidence [16,17] that the angular correlation of these collisions away from threshold are highly dependent upon the target. Only one previous measurement [5] for angular correlation of e-H ionization (1 eV above threshold in the coplanar geometry) can be considered to be substantially within the Wannier region.

We now report several significant experimental developments. The present work extends the observable energy of the escaping electrons down to 0.05 eV and reports simultaneous measurements of double- and triple-differential cross sections, also made simultaneously over a wide range of angles and energies. This is made possible by the improved precision and accuracy of a unique single-toroidal electrostatic energy analyzer. We observe in the perpendicular scattering plane where the cross section are about 10 times smaller than coplanar measurements. This instrument avoids many instrumental uncertainties, particularly, for example, the different alignments and transmission and detection efficiencies which are inherent in the use of separate rotatable energy analyzers for two or more scattered electrons when sequential rather than simultaneous observations are made. We demonstrate these features for six experimental aspects, each with significant physical consequences.

The basic experiment uses a conventional crossed electron-atom beams apparatus, but with a new high-efficiency toroidal electrostatic electron-energy analyzer, shown in Fig. 1. A detailed description of the instrument [18] and its initial application to the measurement of triple-differential $(e, 2e)$ cross sections for the separated fine-structure states of krypton [19] have been reported previously. However, here we describe a new and significant

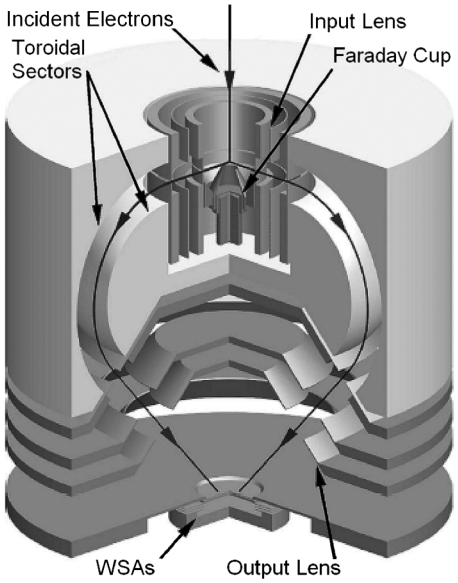

FIG. 1. Schematic diagram of the 360° electrostatic toroidal electron-energy analyzer.

mode of operation of the instrument that makes this study possible. We now discuss six features of the analyzer that are significant for the present study.

(i) The analyzer gives continuous energy and angular distributions over wide ranges in a single scattering plane. Alternate use of a continuous angular distribution is sampled with annular exit slits and a continuous energy distribution is sampled by radial slits. Regions of interest are selected by either physical entry and exit slits or computer software for efficient data collection. We used either 9, 12, or 18 sector-shaped slits, with centers separated by 10°, 15°, or 20°, respectively, and arranged with half the slits on each ''wedge-and-strip'' anode (WSA) [18].

(ii) Electrons that pass through the analyzer and exit slits are focused onto 40 mm diameter microchannel plates (MCPs) whose output charges are collected by each of the three electrodes of two separate WSAs, each covering a semicircular half of the MCPs [18]. Coincidence signals are obtained between the two halves for any location. Charge-sensitive preamplifiers from each of the three electrodes of each WSA give both the fast timing and the location of the incident electrons and this gives perfect correlation between them. This significant feature is in marked contrast to the usual resistive anode position-sensing device which required the timing identification from the charge pulse from the output of the second channel plate multiplier and which is usually limited to less than 95% correlation between timing and position identification. In this way the two electrons from a single scattering event are identified.

(iii) The present study takes advantage of perpendicular-plane (with polar angles of 90°) scattering for which the Legendre polynomials for odd states of total angular momentum are zero so p and f waves (and so on) do not contribute to the observed signal.

(iv) By appropriate selection of the operating mode of the analyzer, the full energy range of the scattered electron can be dispersed across, and contained within, the output slit. Hence double-differential cross sections (DDCSs) can be measured. Thus coincidences between any two sectors [see item (i)], or points on the sectors, determine triple-differential cross sections (TDCSs); the signal from any angle can be summed over energies to give a DDCS (with respect to angle) or over angles to give a DDCS (with respect to energy), and finally summing over all radii (energies) and angles to give a single-differential cross section (SDCS). Here we do not give a SDCS since there would be only a single number. Similarly for future work, we note that rotating the incident-electron beam angle gives other SDCSs and so on, while the insertion of a total ion collector gives a TICS.

(v) Since the singles count rates must be isotropic in the perpendicular plane, any variations in gain across the MCP detectors could be compensated for accurately. Similarly, all pairs of entry and exit slits with the same separations should give the same count rate, within statistical uncertainty. Since only a single-toroidal electrostatic field disperses the analyzed electrons, the energy and angular calibrations and alignment are guaranteed to be constant in contrast to rotatable analyzers.

(vi) The use of a single analyzer for the two outgoing electrons gives only a single set of experimental uncertainties for the outgoing electrons, rather than two sets when separate analyzers are used. Thus, the uncertainties introduced from different acceptance solid angles, energy calibrations, detection efficiencies (other than across the MCPs), energy resolution, and time variation for sequential measurements are eliminated.

Apart from the toroidal spectrometer, the experiment is based on a conventional $(e, 2e)$ crossed beams apparatus. Typical operating characteristics were, for example, a 20 eV incident-electron beam with about 3 μA in a diameter of 0.5 mm and beam angle of about 0.5° and analyzer energy dispersion up to 7 eV. However, these characteristics varied widely for other incident and analyzed energies as may be deduced from Figs. 2–4.

The experimental data were compared with numerical solutions of the full Schrödinger equation. We used the propagating exterior complex scaling (PECS) method [20] to compute solutions in a finite but extended region of coordinate space, typically out to a hypersphere of sufficient radius to ensure the asymptotic form of the ionization wave function could be reliably assumed. A surface-integral technique was used to evaluate the ionization amplitudes from these wave functions. Details of this method are given in [20,21], and it has been shown to provide accurate results near ionization threshold [14]. This method is an adaptation of the exterior complex

scaling technique pioneered by McCurdy *et al.* [22]. Different numerical algorithms are used in PECS to ensure solutions can be obtained very close to threshold. The present calculations were undertaken at incident-electron energies ranging from $E_0 = 14.1$ to 20.4 eV, with grid sizes and maximum partial-wave angular momentum of $R_0 = 180$ to $100a_0$ and $L_{\max} = 6$ to 10, respectively.

The measured data have a statistical uncertainty of about 10% and have been normalized at 14.6 eV at $\phi_{12} = 180°$ to the PECS calculated values. The smallest measured separation between electrons was $\phi_{12} = 60°$ and the lowest incident energy was 14.1 eV. The electrons were accelerated from the first aperture up to the pass energy of the analyzer and great care had to be taken to minimize stray electrons from around the interaction region. An absolute cross section calibration was also made at this energy, yielding a value 6% higher than the calculated PECS value, with uncertainty $\pm 15\%$. The absolute calibration procedure is well known and is discussed by Williams [23] and references therein. The absolute measurements were not used for these comparisons as it would not add to the worth of the study. The estimated standard error of the TICS of the PECS calculations range from 3% at 14.1 eV to 1% at 20.4 eV.

In Fig. 2 we show symmetric ($E_1 = E/2$) and highly asymmetric ($E_1 = E/10$) energy sharing TDCSs at total energies of 0.5 and 6.8 eV above ionization threshold (13.6 eV). The small error bars of the asymmetric measurements at $E = 0.5$ eV demonstrates the remarkable performance of the new instrument for measuring the angular correlation of very low-energy (0.05 eV) electrons. They have a Gaussian-like distribution about $\phi_{12} = 180°$ that is relatively independent of energy sharing, which is consistent with Wannier theory [11]. By 6.8 eV above threshold, the Wannier peak has diminished and is dominated by secondary peaks at $\phi_{12} = 104°$ and 256°.

It is interesting to note that the details of the structure of the TDCSs, as we move to higher energies, is quite dependent on the target species. This was noted by Schlemmer *et al.* for the coplanar geometry of H and He targets. Pan and Starace [17] confirmed the measurements using a distorted wave model.

Zhang *et al.* [24] and Murray *et al.* [6] investigated the peak structure of e-He measurements in the perpendicular plane and gave a phenomenological explanation for the collision process; the single peak structure at 180°, which is favored near threshold, is due to a single-collision process and the second peak is due to a double-collision process that is energetically favored away from threshold. The deviations from the Wannier geometry are clearly seen in the hydrogen and helium measurements at higher energies, but important differences are evident. First, for e-He collisions, the double-collision process does not dominate until 50 eV above threshold, and never dominates in the asymmetric-energy sharing manifold [6]. This contrasts with the clear dominance of the double-collision mechanism for e-H collisions at 6.8 eV above threshold. Second, the double-collision peaks in the e-H system are dominant in both asymmetric- and symmetric-energy sharing arrangements, whereas for helium they are much smaller in asymmetric kinematics and merge with and broaden the single-collision peak. Third, the angle of the double-collision peak in e-He is approximately 96°, shifted from our hydrogen result of 104°. So, while the width of the Wannier peak of both targets have been shown to conform to the same $E^{0.25}$ law [2,14] near threshold, their departure from this law with increasing energy is very different.

In Fig. 3 we use the DDCS measurements (with respect to ϕ_{12}) to show in finer detail the transition from Wannier behavior in the near-threshold region with increasing energy, noting that the results are symmetric about $\phi = 180°$ in the perpendicular plane. At 14.1 and 14.6 eV, within 1 eV of ionization threshold, the DDCS exhibits a

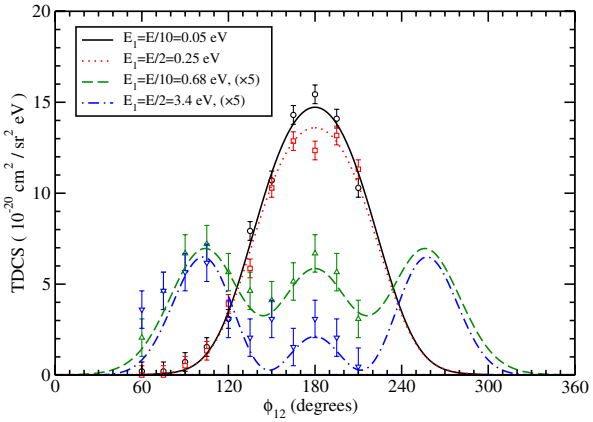

FIG. 2 (color online). Present electron-impact ionization TDCS measurements and calculations for hydrogen as a function of the angle between outgoing electrons (ϕ_{12}) in the perpendicular-plane geometry with polar angle of 90°.

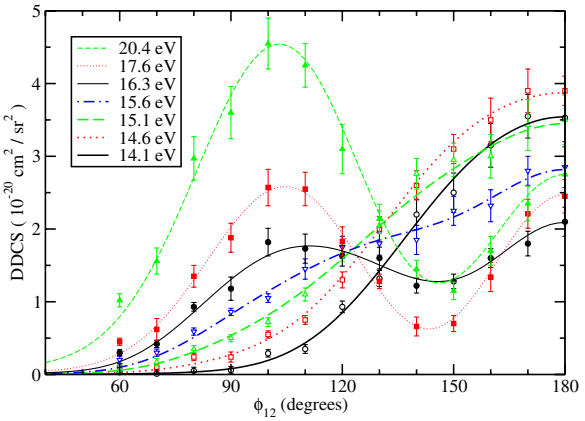

FIG. 3 (color online). Present electron-impact ionization DDCS measurements and calculations for hydrogen for the perpendicular-plane geometry as a function of ϕ_{12}, for various incident energies.

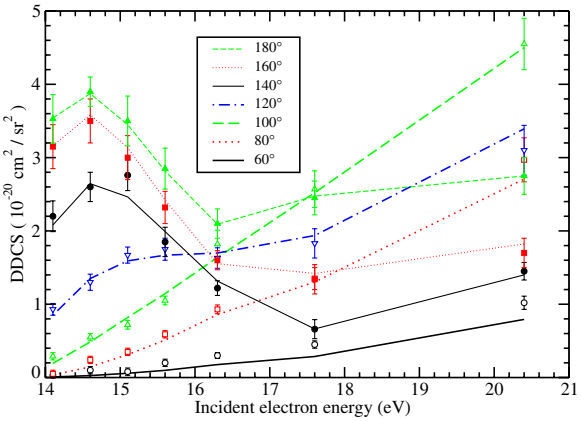

FIG. 4 (color online). The same data as in Fig. 3 but plotted as a function of incident-electron energy for various ϕ_{12}.

Gaussian-like shape centered at 180°. At 15.6 eV the emerging double-scattering peak is clearly evident and becomes dominant above 17.6 eV. The progressive change from a single peak to a double-peak structure suggests that the region of validity of the Wannier model is restricted to less than 2 eV above the ionization threshold for e-H.

Figure 4 shows the DDCS results of Fig. 3 plotted as a function of incident-electron energy for various electron scattering angles. The decreasing dominance of the Wannier contribution to the cross sections at nearly back-to-back angles (180° to 140°) is readily evident with increasing energy. The most interesting feature of this plot is that the DDCS near the double-collision peak (100°) increases linearly with energy above the ionization threshold. Given that the deviation from the Gaussian shape predicted by Wannier theory is shown in Fig. 3 to be due to the evolution of the double-collision peak, this linear dependence confirms that Wannier theory is strictly applicable only *at* ionization threshold.

The PECS calculations in all figures are in excellent agreement with measurement, with the exception of $\phi_{12} = 60°$, where cross sections are relatively small and the PECS results are systematically lower than measurement by 2 standard deviations.

In conclusion, simultaneous measurements using a single-toroidal electrostatic electron-energy analyzer, with improved accuracy and energy range, have revealed the angular dynamics of near-threshold collisions for hydrogen in the perpendicular plane. Double- and triple-differential cross sections were obtained for final-state electrons with energies ranging from 0.05 to 6.8 eV. The PECS calculations are in excellent agreement with the absolute measurements, demonstrating that accurate solutions to the full Schrödinger equation provide a complete description of the collision process near the ionization threshold.

We acknowledge the Australian Research Council and the Australian Partnership for Advanced Computing for research funding and supercomputing facilities.

[1] L. Caron and L. Sanche, Phys. Rev. A **72**, 032726 (2005).
[2] A. Huetz and J. Mazeau, Phys. Rev. Lett. **85**, 530 (2000).
[3] J. Röder, H. Ehrhardt, C. Pan, A. F. Starace, I. Bray, and D. V. Fursa, Phys. Rev. Lett. **79**, 1666 (1997).
[4] J. Röder, M. Baertschy, and I. Bray, Phys. Rev. A **67**, 010702(R) (2003).
[5] J. G. Childers, K. E. James, I. Bray, M. Baertschy, and M. A. Khakoo, Phys. Rev. A **69**, 022709 (2004).
[6] A. J. Murray, M. B. J. Woolf, and F. H. Read, J. Phys. B **25**, 3021 (1992).
[7] M. Schulz, R. Moshammer, D. Fischer, H. Kollmus, D. H. Madison, S. Jones, and J. Ullrich, Nature (London) **422**, 48 (2003).
[8] G. H. Wannier, Phys. Rev. **90**, 817 (1953).
[9] A. Temkin, Phys. Rev. Lett. **49**, 365 (1982).
[10] I. Vinkalns and M. Gailitis, in *Proceedings of the 5th International Conference on the Physics of Electronic and Atomic Collisions*, edited by I. P. Flaks and E. S. Solovyov (Leningrad, Nauka, 1967), pp. 648–650.
[11] A. R. P. Rau, Phys. Rev. A **4**, 207 (1971).
[12] S. Cvejanović and F. H. Read, J. Phys. B **7**, 1841 (1974).
[13] T. N. Rescigno, M. Baertschy, W. A. Isaacs, and C. W. McCurdy, Science **286**, 2474 (1999).
[14] P. L. Bartlett and A. T. Stelbovics, Phys. Rev. Lett. **93**, 233201 (2004).
[15] H. Ehrhardt, M. Schulz, T. Tekaat, and K. Willmann, Phys. Rev. Lett. **22**, 89 (1969).
[16] P. Schlemmer, T. Rösel, K. Jung, and H. Ehrhardt, Phys. Rev. Lett. **63**, 252 (1989).
[17] C. Pan and A. F. Starace, Phys. Rev. Lett. **67**, 185 (1991).
[18] R. W. van Boeyen and J. F. Williams, Rev. Sci. Instrum. **76**, 063303 (2005).
[19] J. F. Williams, R. W. van Boeyen, and S. Samarin, Phys. Rev. A **71**, 052709 (2005).
[20] P. L. Bartlett, A. T. Stelbovics, and I. Bray, J. Phys. B **37**, L69 (2004).
[21] P. L. Bartlett and A. T. Stelbovics, Phys. Rev. A **69**, 022703 (2004).
[22] C. W. McCurdy, M. Baertschy, and T. N. Rescigno, J. Phys. B **37**, R137 (2004).
[23] J. F. Williams, J. Phys. B **14**, 1197 (1981).
[24] X. Zhang, C. T. Whelan, and H. R. J. Walters, J. Phys. B **23**, L173 (1990).